Comprehensive analysis of macrophage-associated inflammatory genes in AMI based on bulk combined with single-cell sequencing data

Xugang Kong[1] and Guangjun Jin[2]

[1] Department of Cardiology, Xiasha Campus, Sir Run Run Shaw Hospital, College of Medicine, Zhejiang University, Hangzhou, Zhejiang, China
[2] Medical Department, The Second Affiliated Hospital of Zhejiang Chinese Medical University, Hangzhou, Zhejiang, China

ABSTRACT

Background. Previous studies have highlighted the crucial role of macrophages in the post-acute myocardial infarction (AMI) inflammatory response. This study specifically focused on investigating macrophage-related targets involved in the inflammatory response after AMI.

Methods. Bioinformatics methods were applied for identifying differentially expressed genes (DEGs) in datasets GSE163465, GSE236374, and GSE183272 obtained from the Gene Expression Omnibus (GEO) database. Communication analysis was conducted to analyze macrophages in AMI. Subsequent analyses encompassed functional enrichment analysis of Co-DEGs using Gene Ontology (GO) and Kyoto Encyclopaedia of Genes and Genomes (KEGG). Gene set variation analysis (GSVA) and immune infiltration analysis were carried out for screening key genes. Validation of the bioinformatics analysis results involved original and GSE114695 datasets, supported by quantitative real time polymerase chain reaction (qRT-PCR). Animal experiments confirmed the upregulation of Saa3, Acp5, and Fcgr4 genes in AMI mouse myocardial tissues.

Results. A total of 80 and 1,907 DEGs were respectively identified by analyzing scRNA-seq and bulk RNA-seq data. The overlapping Co-DEGs were found to be closely associated with inflammation-associated pathways, specifically the PI3K-Akt-mTOR pathway. Screening based on GSVA scores and macrophage-associated scores highlighted four key genes (Saa3, Ms4a4c, Acp5, and Fcgr4). Immunoinfiltration analysis revealed their close association with macrophages. Dataset validation corroborated these findings. Experimental validation focused on Saa3, Ms4a4c, Acp5, and Fcgr4, demonstrating the upregulation of their expression in cardiac macrophages in the AMI group, consistent with previous reports.

Conclusion. This study provides new perspectives on AMI treatment. In addition, Saa3, Acp5, and Fcgr4 exhibit potential as biomarkers for improving cardiac repair and slowing down the development of heart failure after AMI.

Subjects Biochemistry, Bioinformatics, Cardiology
Keywords Acute myocardial infarction, Macrophage, Single-cell sequencing, Bioinformatics analysis, Inflammation

INTRODUCTION

Cardiovascular diseases (CVDs) remain the leading cause of death worldwide, with acute myocardial infarction (AMI) being the majority of such diseases (*Liao et al., 2020*). AMI is mostly characterized by severe and persistent retrosternal pain, and potential complications including cardiac arrhythmia and heart failure, which can lead to catastrophic consequences for human health (*Wang et al., 2023*).

Myocardial remodeling after AMI is closely related to myocardial fibroblasts (*Burke, Burgos Villar & Small, 2021*). Research suggests the active involvement of myocardial fibroblasts in the inflammatory, proliferative, and maturation phases of post-infarction cardiac remodeling with different cellular phenotypes (*Venugopal et al., 2022*).

The inflammatory phase is essential for the progression of myocardial infarction to the reparative and proliferative phases (*Shook, Singh & Singh, 2023*). There is substantial evidence indicating that following AMI, a large number of neutrophils and monocytes rapidly infiltrate into the infarcted area and release proinflammatory cytokines to induce macrophage aggregation, which contribute to the occurrence of post-infarction inflammatory response (*Wang, Chen & Zhang, 2023*).

Studies have shown that MI-like macrophages reduce the angiogenic capacity of endothelial cells, exacerbate myocardial injury, and inhibit cardiac healing. M2 macrophages generate proangiogenic factors to promote angiogenesis and tissue healing (*Liu et al., 2020*). Additionally, *Li et al. (2021)* found that hypoxia exacerbates myocardial infarction injury by promoting macrophage conversion to a repair phenotype. Thus, macrophages are important in the post-AMI inflammatory response, remodeling and repair processes. Identifying novel targets for regulating macrophage function presents a promising avenue for treating myocardial remodeling following AMI (*Cai et al., 2023*).

In this study, different analytical methods were respectively applied for analyzing the bulk RNA data and single-cell data to obtain common genes, which were subsequently validated in a mouse model. The objective was to enhance the identification of AMI-related key genes and targets in the inflammatory response by exploring the differences in the expression of macrophage-related targets in AMI mice through analysis of scRNA-seq data and bulk RNA-seq data.

MATERIAL AND METHODS

Data collection

Single-cell data were collected from the GSE163465 dataset in the Gene Expression Omnibus (GEO) database (https://www.ncbi.nlm.nih.gov/geo/). This dataset consists of one sample from mice in the AMI group and one sample from mice in the Sham group. Bulk data were collected from the GSE236374 and GSE183272 datasets in the GEO database. The GSE236374 dataset contains three healthy Sham samples and three samples with AMI. The GSE183272 dataset contains five samples with AMI and five healthy Sham samples. The GSE114695 dataset includes six healthy Sham samples and six samples with AMI. Healthy samples from the dataset and samples from day seven after AMI were used for this study.

Cell clustering analysis

Nineteen cell clusters were obtained after UMAP dimensionality reduction clustering of single-cell data (GSE163465) using the Seurat package (v 4.3.0.1) and cell-type annotation using the SingleR package (v 2.2.0).

Identification of AMI-associated differentially expressed genes (DEGs)

To identify AMI-associated DEGs, differential analysis was conducted on samples from the training dataset using the FindMarkers function in the Seurat software package. The established thresholds were set at p-value <0.05 and $|log2FC|>0.5$.

Analysis of intercellular communication

To understand the AMI network, the CellChat software package (v 1.6.1) was used to assess the strength and probability of cell–cell communication in AMI mice. Circle plots were used to show the number and strength of interactions between any two cell types within each cellular signaling pathway. Subsequently, the strength and contribution of interactions between dominant cells and other cells was further investigated.

Identification of DEGs and Co-DEGs

All the data from the GSE236374 dataset and the GSE183272 dataset were re-normalized using the sva package v3.52.0 for batch effect removal. The threshold of DEG screening was p-value <0.05 and $|log2FC|>0.5$. DEGs ($n = 80$) identified in the Sc-RNA dataset were overlapped with those ($n = 1,907$) identified in the bulk-RNA dataset, forming the Co-DEG for subsequent analysis.

Gene Ontology (GO) and Kyoto Encyclopedia of Genes and Genomes (KEGG) and Wiki pathway enrichment analysis

Enrichment analysis of the Co-DEGs was performed using the DAVID database (https://david.ncifcrf.gov/) and the results obtained were visualized using the ggplot2 package (v 3.4.4), highlighting the pathways ranking in the top list. Likewise, for the top 3 Co-DEGs, all functionally enriched pathways of significantly expressed genes were determined using Wiki pathway databases.

Screening of key genes and immune infiltration analysis

The inflammatory response score for both the AMI and the Sham groups was calculated using the gene set variation analysis (GSVA) algorithm. The key genes related to inflammation-related pathway and macrophage M0 and M2 scores were selected for further analysis. The screened key genes underwent Pearson correlation analysis with genes in inflammatory response pathways to assess the extent of correlation between these key genes and genes associated with inflammation-related pathway.

Validation of the expression of the screened genes in the original datasets

The GSE163465 and GSE236374 datasets were used for gene expression validation. Differential expression of key genes in the AMI and the Sham groups was compared using rank sum test of the ggpubr package (v 0.6.0).

Dataset validation and single-gene Gene Set Enrichment Analysis (GSEA)

The GSE114695 dataset was used for gene expression validation, and GSEA of key genes was conducted using the clusterProfiler package (v 4.8.3; https://bioconductor.org/packages/release/bioc/html/clusterProfiler.html).

Construction of AMI mouse model

Twelve clean-grade SD male mice, weighing 18–22 g each, were purchased from Hangzhou Medical College Laboratory Animal Center. All mice were reared adaptively for two weeks under pathogen-free condition with 20−24 °C and free access to food and water under natural light with day and night. Mice were randomly divided into Sham group ($n = 6$) and AMI group ($n = 6$). Mice were used for constructing AMI model by ligating the left anterior descending (LAD) coronary artery (*Peng et al., 2023*) and anesthetized with 5% isoflurane.The mice heart was exposed by creating a transverse chest incision, and the LAD branch was ligated using a puncture needle in the interventricular groove, approximately 2–3 cm below the left auricle. The myocardium displayed a change in color, becoming white or cyanotic after ligation. Subsequently, the heart was repositioned into the chest cavity, followed by closure of the chest and suturing of the skin. The Sham group mice underwent only thoracotomy without LAD ligation. After 1 week of LAD ligation in mice, the cardiac function in the left ventricle was assessed using M-mode echocardiography. The mice were anesthetized and secured in a supine position on a wooden board. The chest was fully exposed, and the chest fur removed with hair removal cream. An ultrasound instrument was adjusted to display an M-mode echocardiogram. Left ventricular end-diastole diameter (LVEDD), left ventricular end-systolic diameter (LVESD), left ventricular fraction shortening (LVFS), and left ventricular ejection fraction (LVEF) of the mice were collected for each group, which were used to assess the level of the cardiac function of the left ventricles of the mice. At the end of treatment, the mice were euthanized by 5% inhalation of isoflurane and cervical dislocation. The heart tissues of mice were isolated and frozen. All study procedures were approved by Institutional Animal Care and Use Committee of Zhejiang Center of Laboratory Animals (NO. ZJCLA-IACUC-20010546).

Calculation of myocardial infarct area in mice by triphenyltetrazolium chloride (TTC) staining

Surviving mice were euthanized through cervical dislocation 1 week after successful AMI modeling. Following anesthesia for blood sampling from the abdominal aorta, fresh hearts were removed, thoroughly washed with saline, and then placed in a refrigerator at −20 °C for about 20 min. Afterward, the hearts were removed from the refrigerator, sliced into 2–3 mm-thick slices and placed in 2% TTC staining solution prewarmed at 37 °C. After 15 min of staining, it was observed that the infarcted area of the mouse heart appeared white, whereas the non-infarcted area was red. Image J (v 1.51 J8) was used for analysis. The percentage of the white infarcted area to the whole section area was used as an index.

Table 1 Primer sequence.

Gene	Oligonucleotide sequence
mmu-Saa3-F	ACATGGAGCAGAGGACTCAAGAG
mmu-Saa3-R	AGCAGGTCGGAAGTGGTTGG
mmu-Ms4a4c-F	TGGGTTCACAGTTTCCGTTTCG
mmu-Ms4a4c-R	AAGCAGAGATGGACACAGCAATG
mmu-Fcgr4-F	TCAGGGTGCTTGAGGAAGACAG
mmu-Fcgr4-R	GTGGGATGAGGCTTTCGTTATGG
mmu-Acp5-F	AGCGACAAGAGGTTCCAGGAG
mmu-Acp5-R	GTTTCCAGCCAGCACATACCAG
mmu-GAPDH-F	ACGGCAAGTTCAACGGCACAG
mmu-GAPDH-R	CGACATACTCAGCACCAGCATCAC

Detection of related gene expression in mouse cardiac macrophages by quantitative reverse transcription polymerase chain reaction (qRT-PCR)

The method for isolating mouse macrophages involved excising the mouse hearts, washing the hearts with heated Hanks Balanced Salt Solution (HBSS) to remove blood, preparing cell suspensions through chopping, homogenizing and digesting, discarding the supernatant after centrifugation, and lysing erythrocytes with ACK lysis buffer (A10492-01; Gibco). After washing, the cells were resuspended in 2 ml HBSS and incubated with 50 ul anti-CD45 (mouse) magnetic beads (Miltenyi 130-052-301) for 30 min. Subsequently, cells were passed through the MACS magnetic column with magnets in place. The column was rinsed with buffer, and labeled cells were eluted for RNA collection (*Carlson et al., 2017*).

Transfection efficiency was determined using qRT-PCR (*Zhang et al., 2020*). RNA from mouse cardiac macrophages in both the AMI and the Sham groups were extracted using Trizol solution (15596026; Thermo Fisher Scientific, USA) and reverse transcribed into cDNA (RR037Q; Takara, Beijing, China). The expression levels of Saa3, Ms4a4c, Fcgr4, and Acp5 were detected using qPCR (CN830S, Takara) with the following reaction conditions were 95 °C for 10 min, 95 °C for 30 s, 60 °C for 30 s, and 72 °C for 1 min, for a total of 40 cycles. The expression levels of Saa3, Ms4a4c, Fcgr4, and Acp5 were calculated using the $2^{-\Delta\Delta ct}$ method. GAPDH was used as the internal marker gene. The primer sequences were designed as follows (Table 1).

Statistical analysis

Statistical analysis was conducted using the R program (v 4.0.2; *R Core Team, 2020*). Data for different genes in the two groups were compared using t-test with GraphPad Prism (v 10.1.0) software, with $P < 0.05$ considered statistically significant.

RESULTS

Analysis of scRNA-seq data

Single-cell data from the GSE163465 dataset were subjected to Uniform Manifold Approximation and Projection (UMAP) dimensionality reduction, revealing 19 different
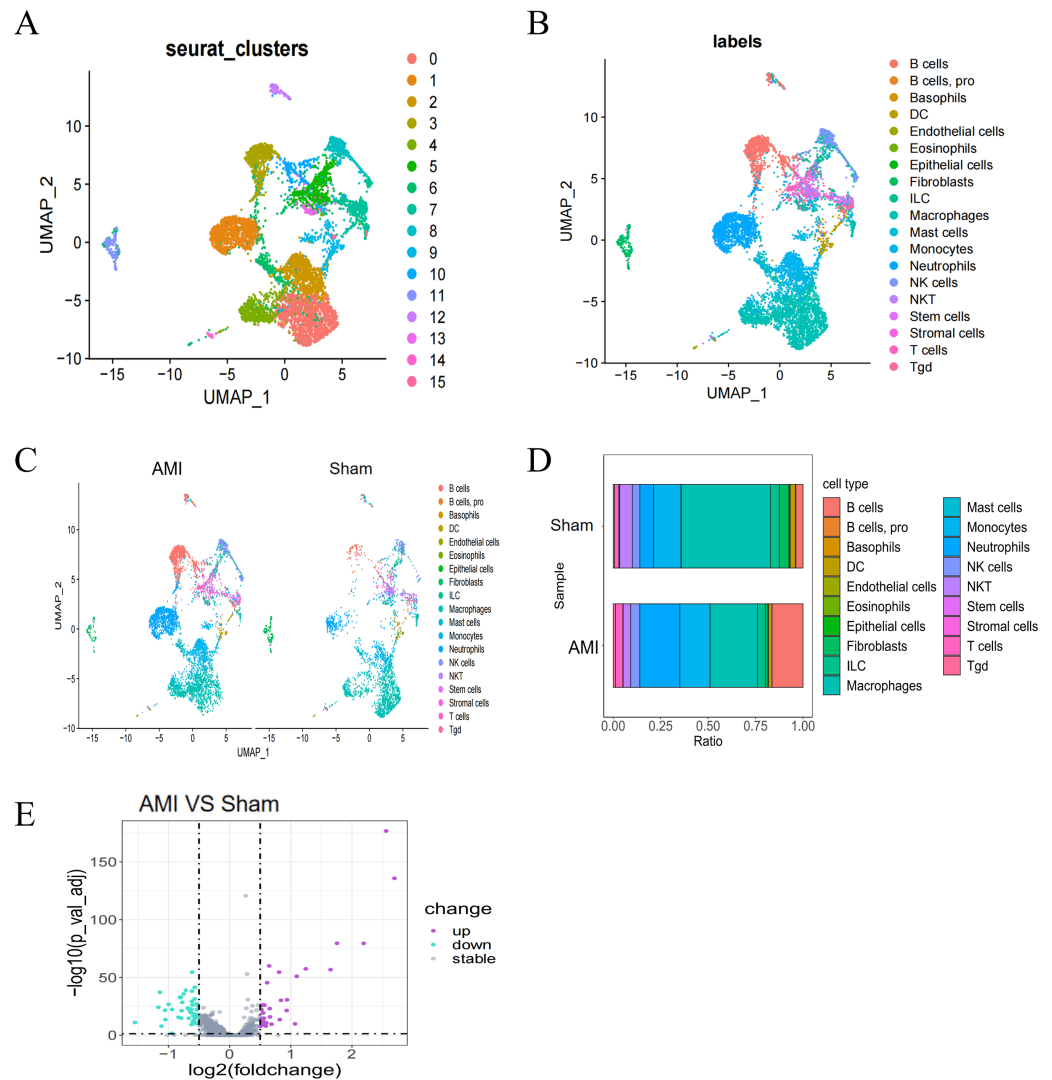
Figure 1 **Single-cell cluster analysis in the AMI and the Sham groups.** (A, B) UMAP plots of cell types in the GSE163465 dataset. Each dot represents a cell nucleus colored by its cell type identity; (C) UMAP plots of cell types in the AMI and the Sham groups; (D) percentage change and contribution of each cell type in the AMI and the Sham groups; (E) volcano plot of DEGs between the AMI and the Sham groups. Purple dots indicate significantly up-regulated genes, green dots indicate significantly down-regulated genes, and gray dots represent genes with no statistical difference.

Full-size ⬚ DOI: 10.7717/peerj.17981/fig-1

clusters in the AMI group, including B cells, basophils, and macrophages (Figs. 1A, 1B). Analysis of the percentage of each cell type in the AMI group compared to the Sham group indicated obvious differences in the percentage of different clusters between the two groups (Fig. 1C, Fig. 1D). DEG analysis on the GSE163465 dataset revealed a total of 80 DEGs between the AMI and the Sham groups, as shown in the volcano plots. (Screening criteria: threshold adjP<0.05, and |$\log_2$FC|>0.5) (Fig. 1E).
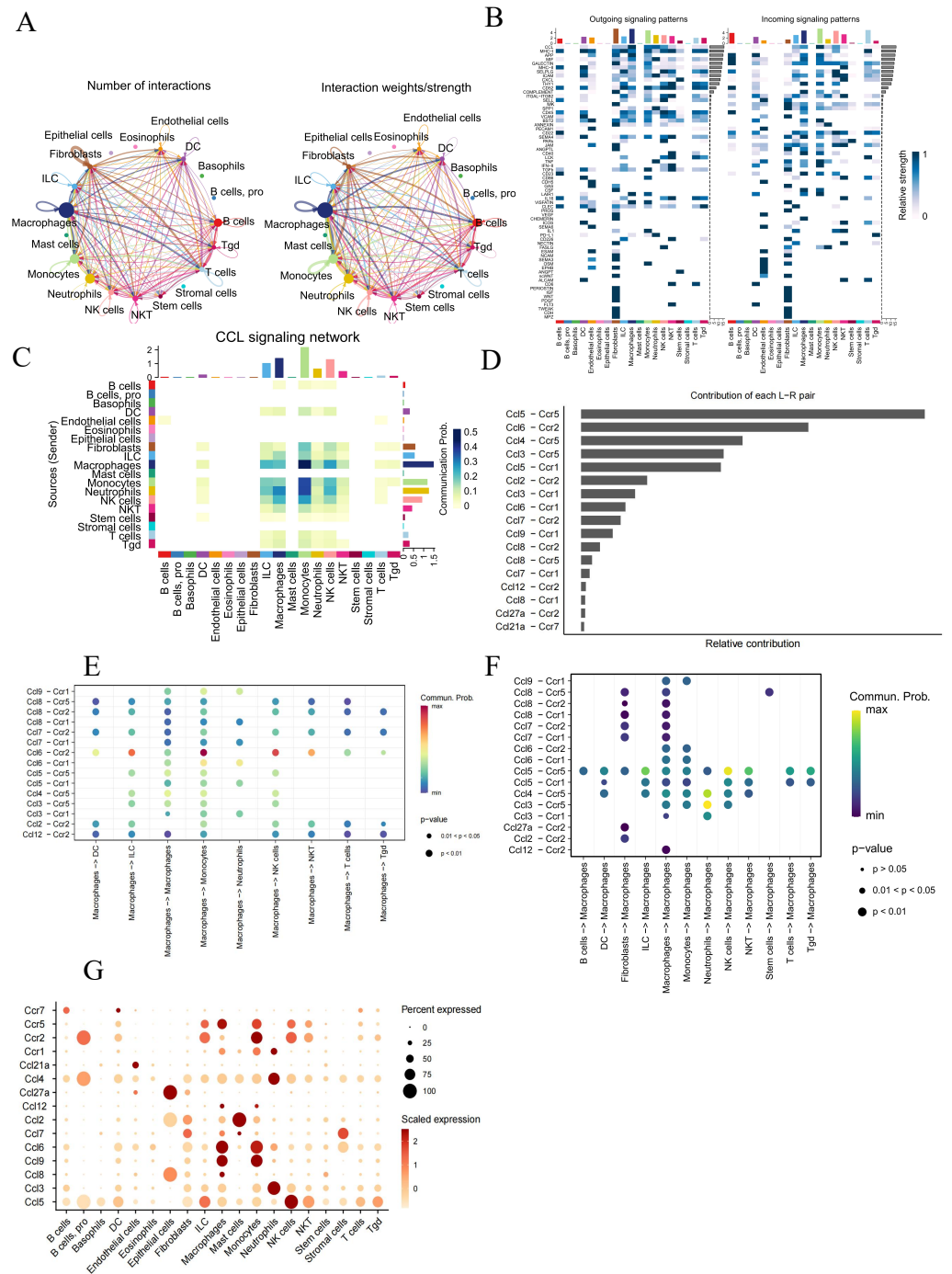
Figure 2 Analysis of intercellular communication in AMI. (A) Number and strength of interactions across different cell types; (B) overview of efferent signaling and afferent signaling; (C) heatmap showing the differential number of interactions between different cell clusters in the CCL signaling network , with the X and Y axes representing receptor and ligand cell types, respectively. (continued on next page...)

Full-size ⬚ DOI: 10.7717/peerj.17981/fig-2

Figure 2 (…continued)
The colored bars on the top and right represent the sum of signals received and sent in each cell type, respectively; (D) relative contribution of each ligand–receptor pair to the CCL signaling network. (E, F) comparison of the probability of ligand–receptor pair-mediated communication between macrophages and other cell types; (G) Strength of association between all the cell types and chemokines.

Analysis of intercellular communication in AMI

The CellChat package was used to analyze scRNA-Seq data for understanding potential intercellular communication in AMI mice from the GSE163465 dataset (Fig. 2A, Fig. 2B). Results indicated macrophages as the dominant contributors to cellular communication, closely interacting with many cells,

The CCL signaling pathway was shown to be closely involved in the interaction between macrophages and monocytes (Fig. 2B). Further investigation of the CCL signaling pathway was conducted with CellChat for better undrstanding cell-to-cell communications (Fig. 2C). Ccl6-Ccr2 and Ccl5-Ccr5 were identified as the main contributor of Ligand-Receptor (L −R) for the CCL signaling pathway. (Fig. 2D). In addition, analyzing the probability of communication for ligand–receptor pairs sent by macrophages to other cell types showed a substantial increase in Ccl 6-Ccr 2 from macrophages to monocytes, and in Ccl 4-Ccr 5 and Ccl 3-Ccr 5 from neutrophils to macrophages (Figs. 2E, 2F). The expression of chemokines and chemokine receptors on the major cell types was further investigated, revealing that the chemokines ccl6 and ccl9 and the chemokine receptor ccr5 can function in macrophages (Fig. 2G).

Functional enrichment analysis of intersecting Co-DEGs

In the analysis of T bulk sequencing data from the GSE236374 and GSE183272 datasets, DEGs between the AMI and the Sham groups were identified. With thresholds of p-value <0.05 and $|log2FC|>0.5$, a total of 1,907 DEGs were discovered, of which 33 overlapped (Fig. 3A). Venn diagrams comparing DEGs from bulk RNA-seq data and scRNA-seq data revealed 33 Co-DEGs (Fig. 3B). Heatmap visualization of the Co-DEGs demonstrated significant differences in their distribution between the AMI and the Sham groups (Fig. 3C). GO and KEGG analyses were respectively performed on the Co-DEGs. GO analysis showed their main involvement in biological processes (BPs) such as regulation of locomotion and regulation of immune system process (Fig. 4A), cellular components (CCs) including fibrinogen complex, plasma lipoprotein particles (Fig. 4B), and molecular functions (MFs) relating to extracellular matrix binding and extracellular matrix structural composition (Fig. 4C). KEGG enrichment analysis demonstrated their involvement in pathways such as amoebiasis, AGE-RAGE signaling pathway in diabetic complications, *etc* (Fig. 4D). Wiki pathway analysis showed predominant enrichment of the,Co-DEGs in the inflammatory response pathway, spinal cord injury, and adhesion foci: PI3K-Akt-mTOR signaling pathway (Fig. 4E).

Screening for macrophage-associated key genes

Inflammatory pathway-related genes were significantly enriched in AMI compared to the Sham group (Fig. 5A). Taking the inflammation-related pathway and macrophage M0 and
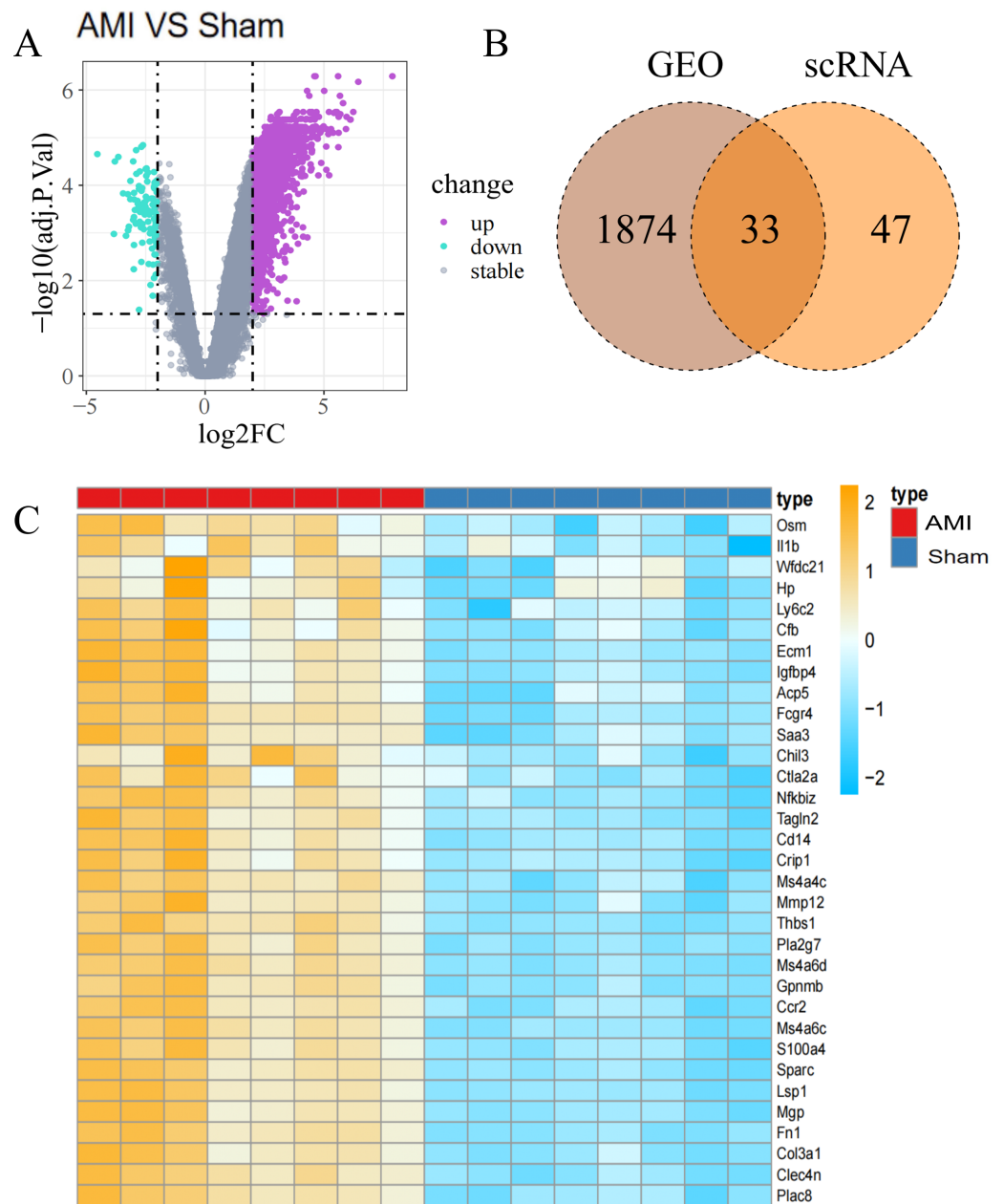
Figure 3 **Identification of Co-DEGs.** (A) Volcano plot of DEGs between the AMI and the Sham groups in bulk RNA-seq data. Purple dots signify significantly up-regulated genes, green dots represent significantly down-regulated genes, and gray dots denote genes with no statistical difference; (B) Co-DEGs obtained by intersecting DEGs from bulk RNA-seq data and scRNA-seq data; (C) heatmap depicting the expression of Co-DEGs in the AMI and the Sham groups, with the yellow part representing a positive correlation and the blue part representing a negative correlation.

Full-size 🖼 DOI: 10.7717/peerj.17981/fig-3

M2 score as conditions, Saa3, Ms4a4c, Acp5, and Fcgr4 were screened out as key genes (Fig. 5B). The relationship between these 4 genes and specific inflammatory response pathway-related genes was displayed (Fig. 5C).
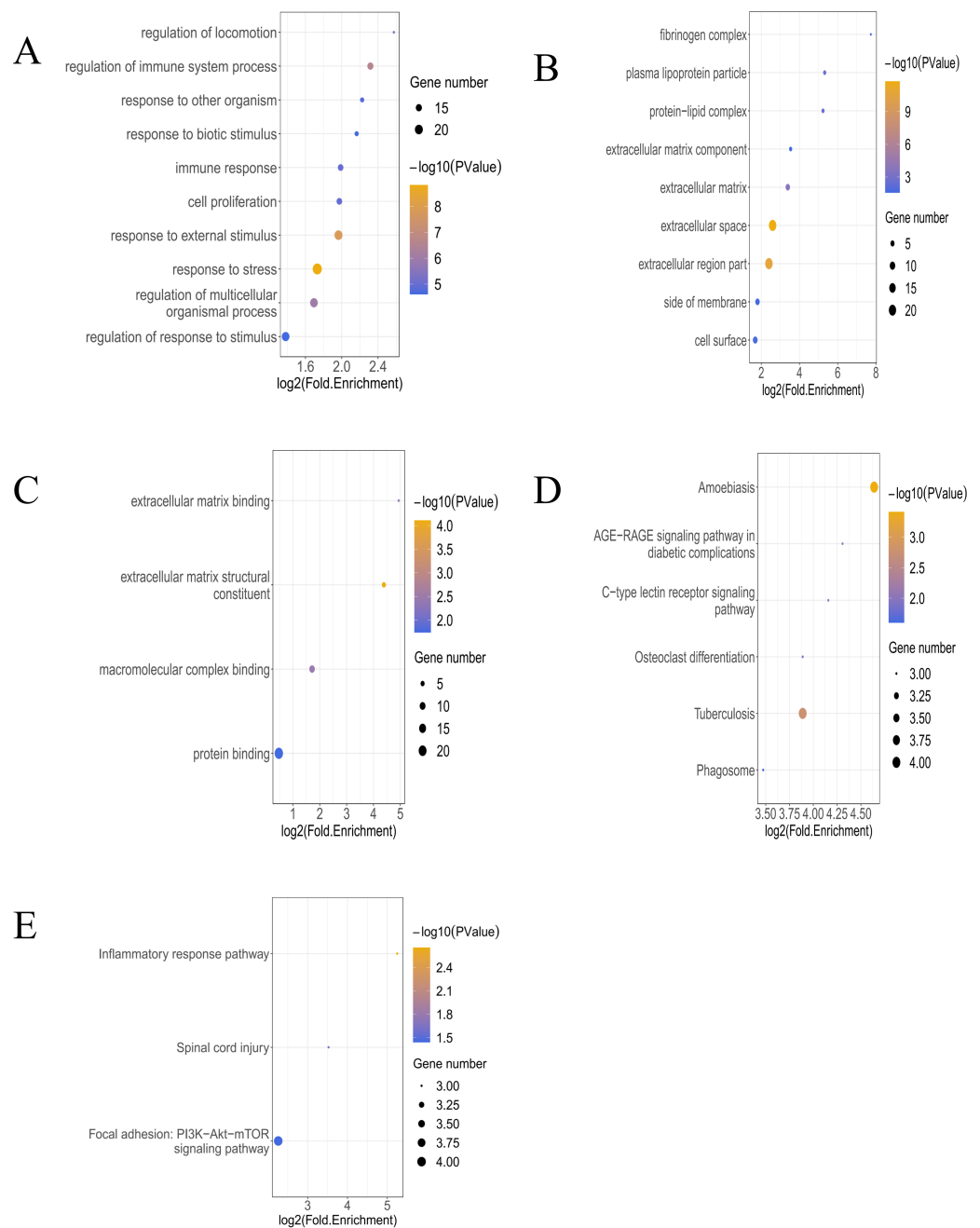
Figure 4 Functional enrichment analysis of Co-DEGs. (A) Bubble diagram illustrating GO-BP results of Co-DEGs. (B) Bubble diagram presenting GO-CC results of Co-DEGs. (C) Bubble diagram displaying GO-MF results of Co-DEGs; GO, gene ontology; BP, biological process; CC, cellular component; MF, molecular function; (D) bubble diagram showing KEGG pathway analysis results of Co-DEGs; KEGG, kyoto encyclopedia of genes and genomes; (E) Wikipathway enrichment analysis of Co-DEGs.

Full-size ▢ DOI: 10.7717/peerj.17981/fig-4
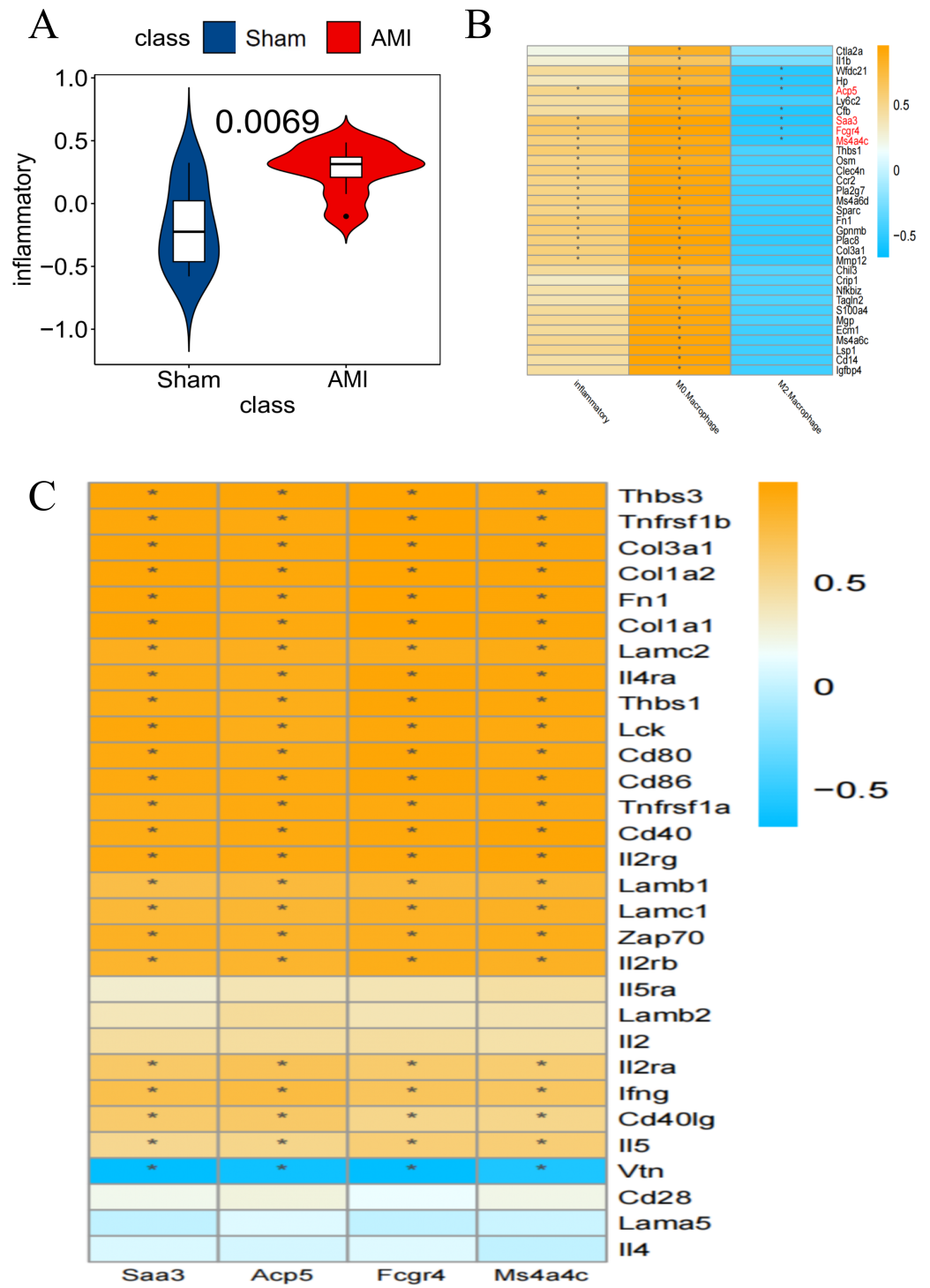
Figure 5 Screening for key genes (A) GSVA scores of Co-DEGs and inflammation-related pathways, with the *Y*-axis representing the association between Co-DEGs and inflammation-related genes; (continued on next page...)

Full-size ⬜ DOI: 10.7717/peerj.17981/fig-5

Figure 5 (...continued)
(B) Co-DEGs significantly related to the specific inflammatory response pathway were selected for further analysis; (C) relationship between key genes and genes associated with specific inflammatory response pathways (*p<0.05). (B–C) The yellow part represents a positive correlation and the blue part represents a negative correlation.
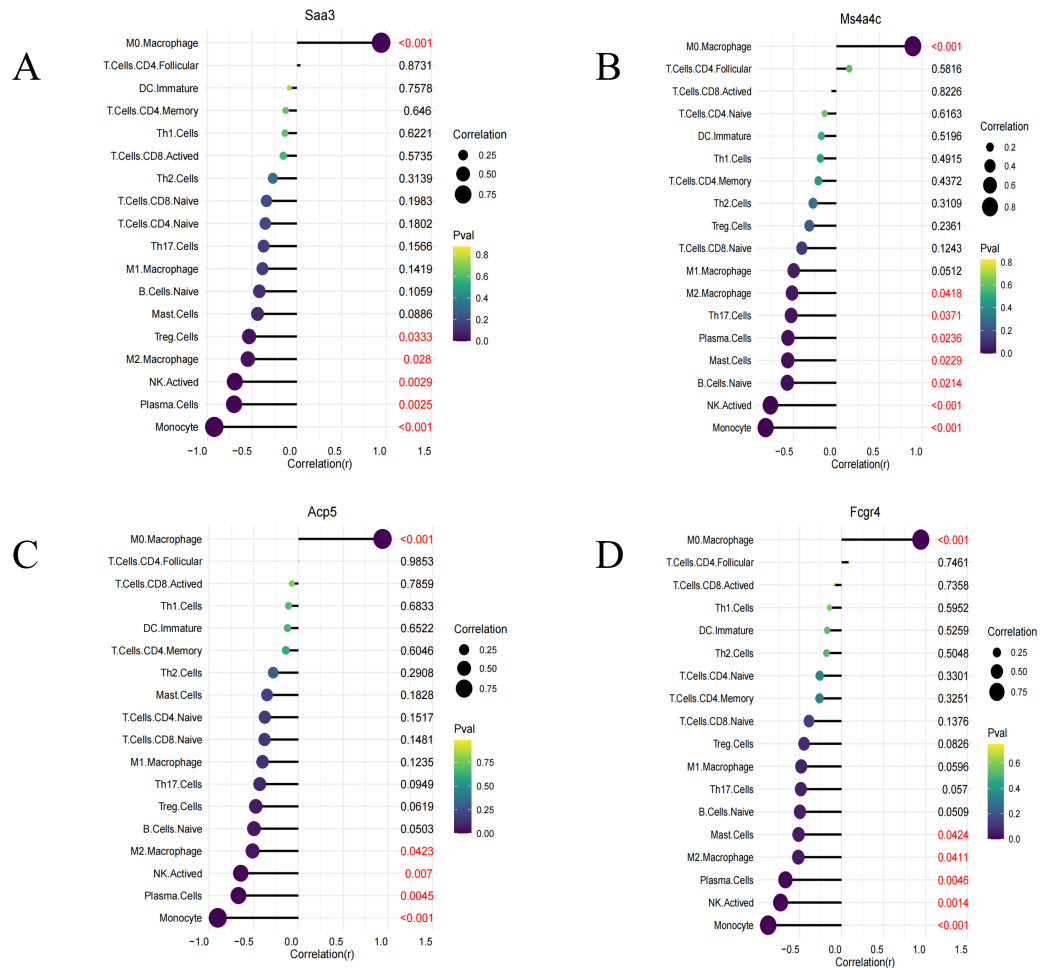

Figure 6 **Immune infiltration lollipop plot.** (A) Correlation map of Saa3 with infiltrating immune cells; (B) correlation map of Ms4a4c with infiltrating immune cells; (C) correlation map of Acp5 with infiltrating immune cells; (D) correlation map of FCGR4 with infiltrating immune cells.

Full-size 🖼 DOI: 10.7717/peerj.17981/fig-6

Immune cell correlation analysis of macrophage-associated key genes

Immune infiltration analysis was performed on the four identified key genes (Saa3, Fcgr4, Acp5, and Ms4a4c). All of them were all positively correlated with M0 macrophages and negatively correlated with M2 macrophages, NK cell stimulation, and others (Figs. 6A–6D).

Validation of the expression of the four screened genes in different datasets

The analysis of the GSE163465 dataset revealed high expression of the key genes (Saa3, Ms4a4c, Fcgr4, and Acp5) in macrophages and monocytes in AMI (Figs. 7A–7D). Additionally, these same genes exhibited significantly high expression in AMI compared to the Sham group in the bulk RNA-seq dataset (Figs. 7E–7H). The validation results from the scRNA-seq dataset exhibited a consistent pattern with the bulk RNA-seq dataset.

Data set validation and GSEA

Analysis results from the GSE114695 dataset demonstrated a notable increase in the expression of all the four key genes in the AMI group compared to the Sham group (Figs. 8A–8D). GSEA results revealed that Saa3 was enriched in the cytokine-cytokine receptor interaction pathway (Fig. 8E), while Ms4a4c, Acp5, and Fcgr4 were significantly enriched in the Salmonella infection pathway (Figs. 8F–8H).

Cardiac function assessment of mice within the constructed AMI model

After 1 week of LAD coronary artery ligation in mice, the cardiac function in the left ventricle was assessed using M-mode echocardiography. Compared with the Sham group, mice in the AMI group developed cardiac systolic and diastolic dysfunction, as indicated by a significant decrease in ejection fraction (EF), fractional shortening (FS), along with an increase in LVESD (Fig. 9).

Assessment of infarct size in AMI mice

After 1 week of successful AMI modeling, the infarct area in mouse hearts was measured. The AMI group exhibited increased and much larger infarct area compared with the Sham group (Fig. 10A), confirming the successful AMI modeling.

Expression validation of 4 key genes by qRT-PCR

Validation of the expression of Saa3, Ms4a4c, Fcgr4, and Acp5 was conducted using qRT-PCR. The results revealed a significant up-regulation of in cardiac macrophages in the AMI group compared to the Sham group, while no significant difference was observed in the expression of MS4A4C between the Sham and AMI groups (Figs. 11A–11D).

DISCUSSION

AMI is a common cardiovascular disease characterized by partial or total obstruction of the coronary arteries, resulting in localized necrosis of a portion of the myocardium due to persistent ischemia and hypoxia (Algoet et al., 2023). AMI is the leading cause of cardiovascular disease morbidity and mortality worldwide, and has been called one of the "top killers" of human health. Excessive immune responses by M1 macrophages can lead to chronic inflammation and inflammatory diseases (Challa et al., 2024), whereas M2 macrophages are involved in tissue repair and immunomodulation (Audu et al., 2022). Following myocardial injury, macrophages are recruited to the site of injury to differentiate. The disproportionate ratio of M1/M2 macrophages causes local inflammatory responses
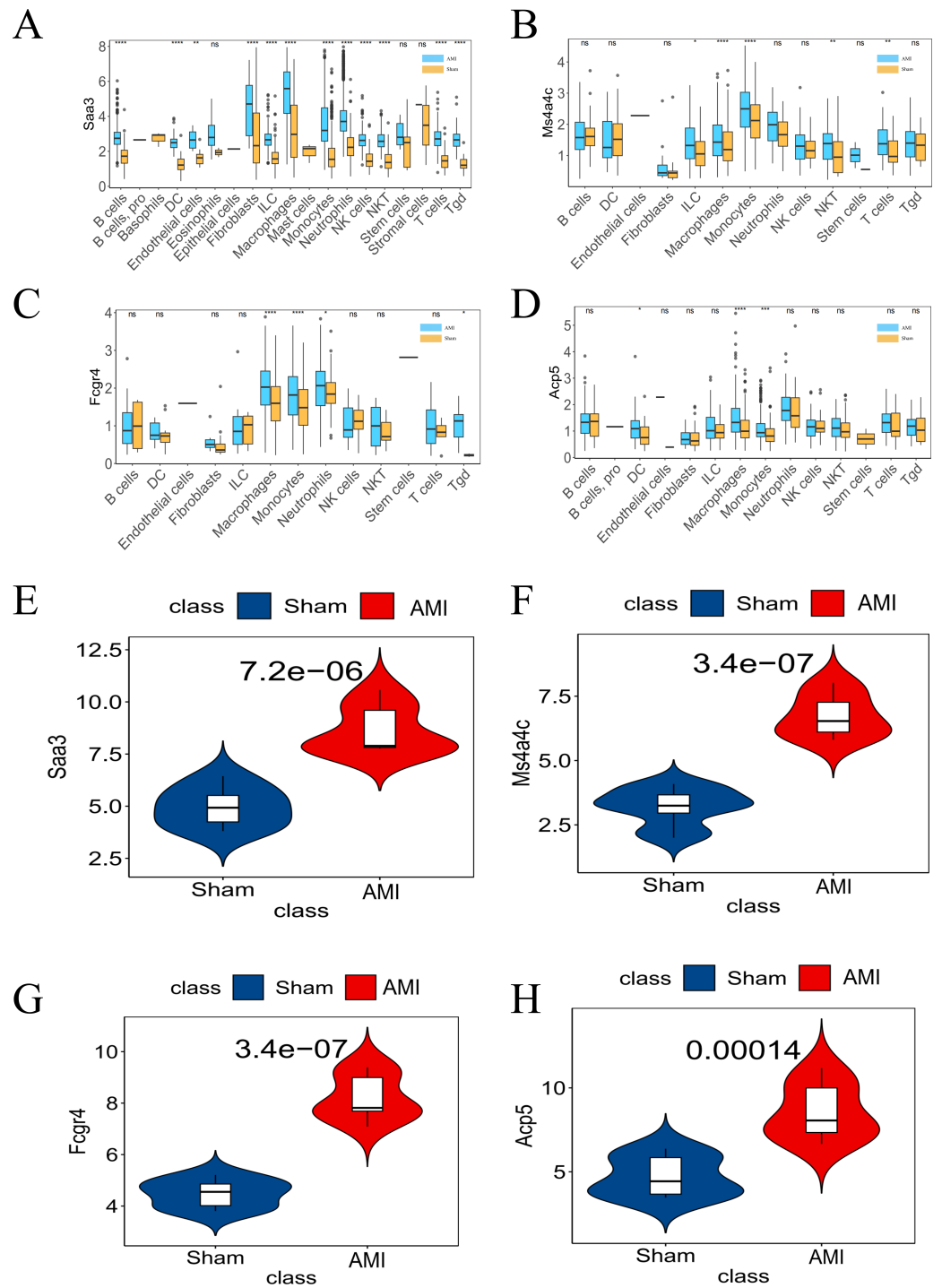
Figure 7 Differential expression of the four key genes between the AMI and the Sham groups. (A) Saa3 expression was analyzed in the GSE163465 dataset; (B) Ms4a4c expression was analyzed in the GSE163465 dataset; (C) Fcgr4 expression was analyzed in the GSE163465 dataset; (D) Acp5 expression was analyzed in the (continued on next page...)

Full-size ☒ DOI: 10.7717/peerj.17981/fig-7

Figure 7 (...continued)
GSE163465 dataset; (E) Saa3 expression was analyzed and validated in the GSE236374 and GSE183272 datasets; (F) Ms4a4c expression was analyzed and validated in the GSE236374 and GSE183272 datasets; (G) Fcgr4 expression was analyzed and validated in the GSE236374 and GSE183272 datasets; (H) Acp5 expression was analyzed and validated in the GSE236374 and GSE183272 datasets. The Y-axis represents the number of different key genes expressed in the cell. (*$p < 0.05$; **$p < 0.01$; ***$p < 0.001$; ****$p < 0.0001$; ns, no significance).

and increased ROS production, leading to myocardial remodeling, which is a major cause of heart failure after AMI (*Lee, Chang & Lin, 2017*).

After AMI, there is a substantial influx of immune cells to the infarcted area, releasing activating cytokines that promote cardiac remodeling. Macrophages play an important role in this process. For instance, interleukin 34 (IL-34) has been identified to enhance CCL2 expression by activating the NF-κB pathway, thereby promoting macrophage recruitment and polarization. This exacerbates cardiac remodeling and heart failure (*Zhuang et al., 2023*). Therefore, it is crucial to delve deeper into the specific mechanisms of myocardial remodeling after AMI and identify macrophage-related targets involved in the post-infarction inflammatory response.

Cell clustering analysis on the GSE163465 dataset revealed significant differences in macrophages between the AMI and the Sham groups. Intercellular communication network analysis highlighted macrophages's highest position in cellular communication, and revealed its close relation to the CCL signaling pathway.

Furthermore, WANG demonstrated that the addition of synthetic o-hyaluronic acid (o-HA) to infarcted tissues also enhanced M2 macrophage polarization through activation of chemokines Ccl2 and CXCL5 (*Wang et al., 2019*).

In this study, 33 Co-DEGs were identified through bioinformatics analysis. They exhibited significant differences between the AMI group and the Sham group, and were mainly enriched in the inflammatory response pathway and the PI3K-Akt-mTOR signaling pathway. The PI3K-Akt-mTOR pathway, known for its wide range of biological effects, plays an important role in mediating cell survival and proliferation (*Jiang et al., 2023*). Previous studies have shown that mTOR overexpression attenuates the inflammatory response in myocardial I/R injury and inhibits cardiac fibrosis (*Lv et al., 2020*). In addition, tanshinone IIA (tanIIA), a lipophilic component of Salvia miltiorrhiza, has demonstrated the ability to suppress inflammation and fibrosis in cardiac tissues *via* the PI3K/Akt/mTOR/eNOS signaling pathway (*Lu et al., 2022*). Gong et al. observed significant changes in p-Akt and p-mTOR in myocardial ischemia/reperfusion injury (*Gong et al., 2021*). The results of the above enrichment analyses suggest that the pathological mechanism of macrophage inflammatory response after infarction is closely related to inflammation mediation, which is consistent with previous studies (*Wei et al., 2023*).

Through GSVA, SAA3, MS4A4C, ACP5, and FCGR4 were identified as key genes highly related to the inflammatory response pathway. Experimental findings showed that mice in AMI group developed cardiac systolic and diastolic dysfunction in comparison to the Sham group. Both qRT-PCR and bioinformatics analysis of cardiac macrophages consistently
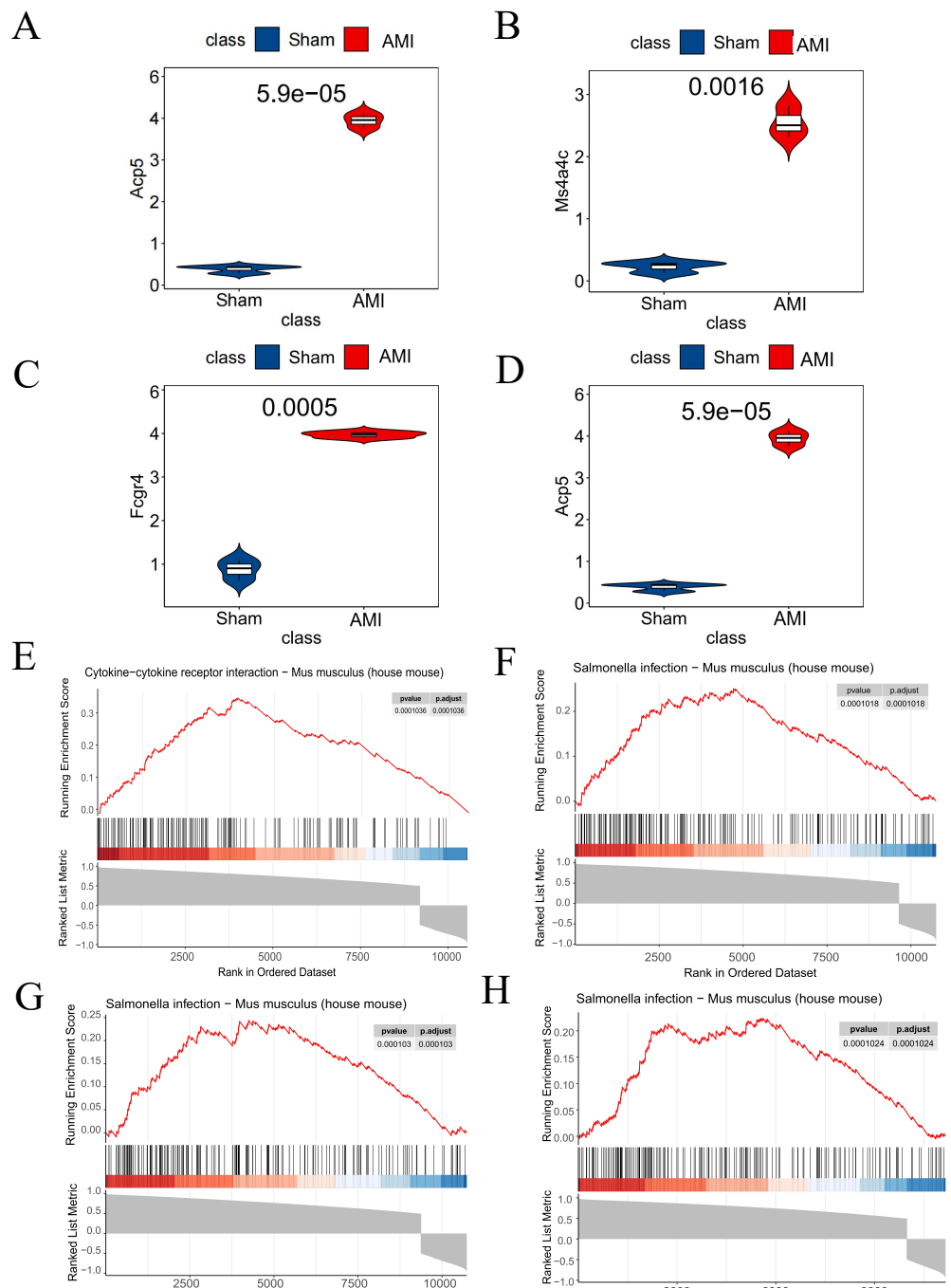
Figure 8 **Dataset validation and GESA.** (A) Saa3 expression validated in the GSE114695 dataset; (B) Ms4a4c expression validated in the GSE114695 dataset; (C) Fcgr4 expression validated in the GSE114695 dataset; (D) Acp5 expression validated in the GSE114695 dataset; (E) GSEA illustrating significant enrichment pathway of Saa3; (F) GSEA illustrating significant enrichment pathway of Ms4a4c; (G) GSEA illustrating significant enrichment pathway of Fcgr4; (H) GSEA illustrating significant enrichment pathway of Acp5; (E) Serine-Cytokine receptor interaction pathway; (F–H) Salmonella infection pathway; GSEA, gene set enrichment analysis.

Full-size 🖼 DOI: 10.7717/peerj.17981/fig-8
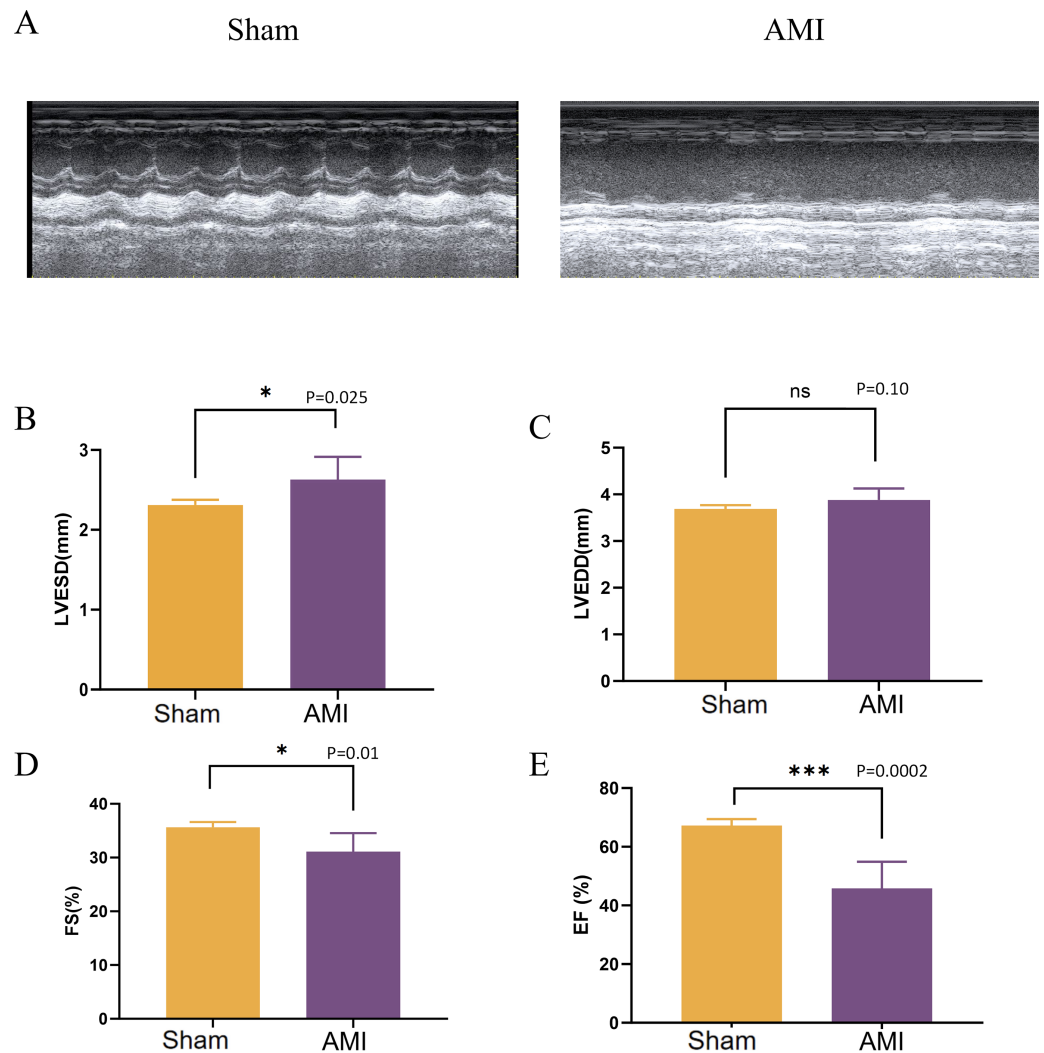
Figure 9 Evaluation of cardiac function 1 week after LAD ligation. (A) M-mode echocardiographic images of mice in the Sham group and 1 week after LAD ligation; (B) LVESD of mice in the AMI and the Sham groups; (C) LVEDD of mice in the AMI and the Sham groups; (D) FS of mice in the AMI and the Sham groups; (E) EF of mice in the AMI and the Sham groups; LVESD, left ventricular end systolic diameter; LVEDD, left ventricular end-diastolic diameter; FS: fractional shortening; EF, ejection fraction. (*$p <$ 0.05; **$p < 0.01$; ***$p < 0.001$; ns, no significance).

Full-size 🖼 DOI: 10.7717/peerj.17981/fig-9

revealed a substantial upregulation of Saa3, Acp5, and Fcgr4 in the AMI group compared to the Sham group.

Serum amyloid A (SAA), primarily secreted by hepatocytes, is expressed at a level of <10 mg/L in the physiological state. However, in response to inflammation and infection stimuli, Hepatocytes markedly increase SAA synthesis and secretion (*Liu et al., 2023*). SAA is an independent risk factor for the occurrence of AMI. The expression level of Saa3 has already been demonstrated as a marker for detecting the level of macrophage infiltration in obese adipose tissue (*Sanada et al., 2016*). Recent reports have shown that Saa3 also promotes atherosclerotic lipid deposition in apoE-/- mice (*Thompson et al., 2018*).
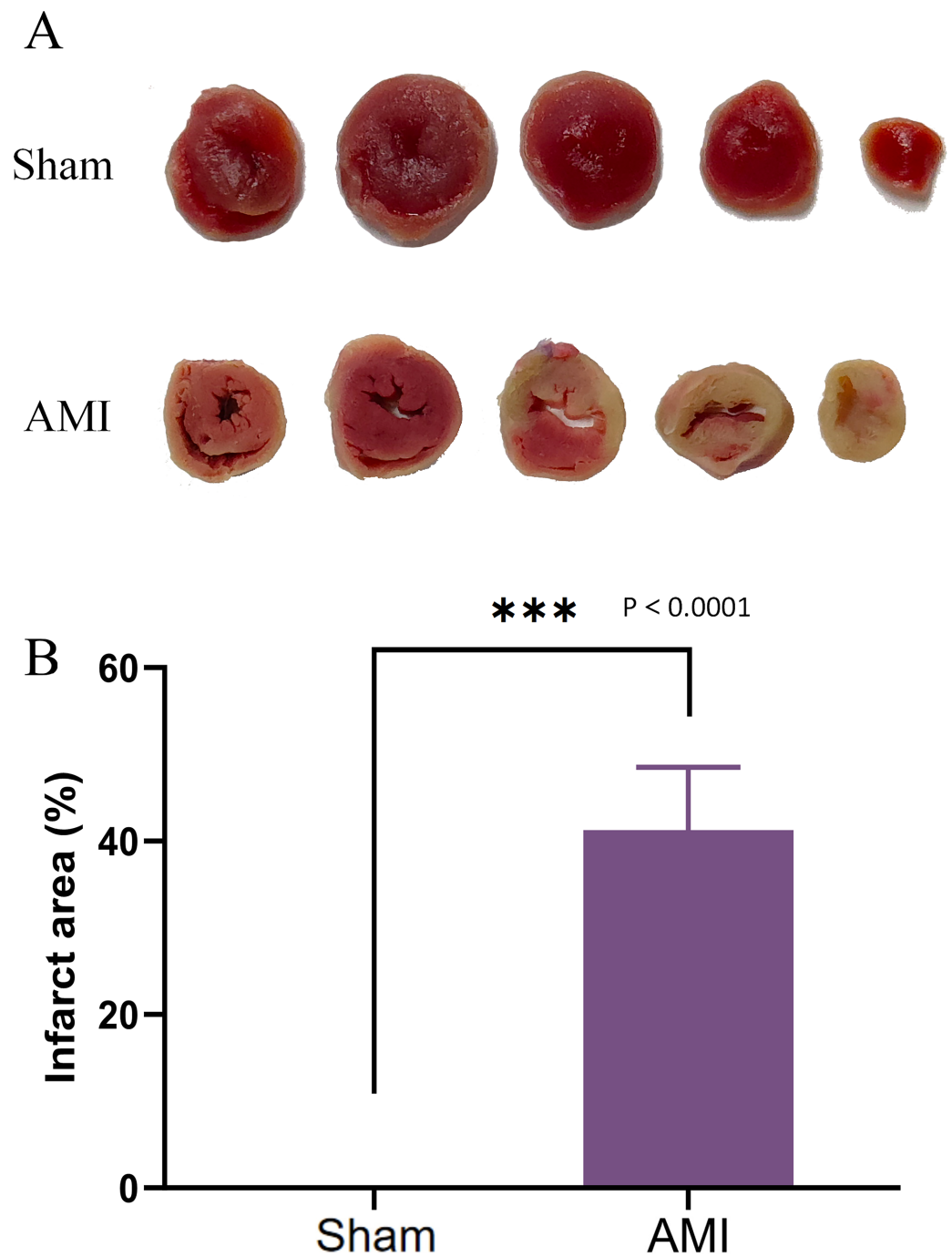
Figure 10 TTC staining of cardiac tissues. (A) Cardiac tissues of mice in the Sham and AMI groups; (B) comparison of myocardial infarction area between the AMI and the Sham groups (***$p < 0.001$).

Full-size ☒ DOI: 10.7717/peerj.17981/fig-10

Tartrate-resistant acid phosphatase 5 (Acp5) is an evolutionarily conserved multifunctional phosphatase involved in skeletal development and regulation of macrophage function (*Ren et al., 2018*). In individuals with chronic inflammatory diseases,
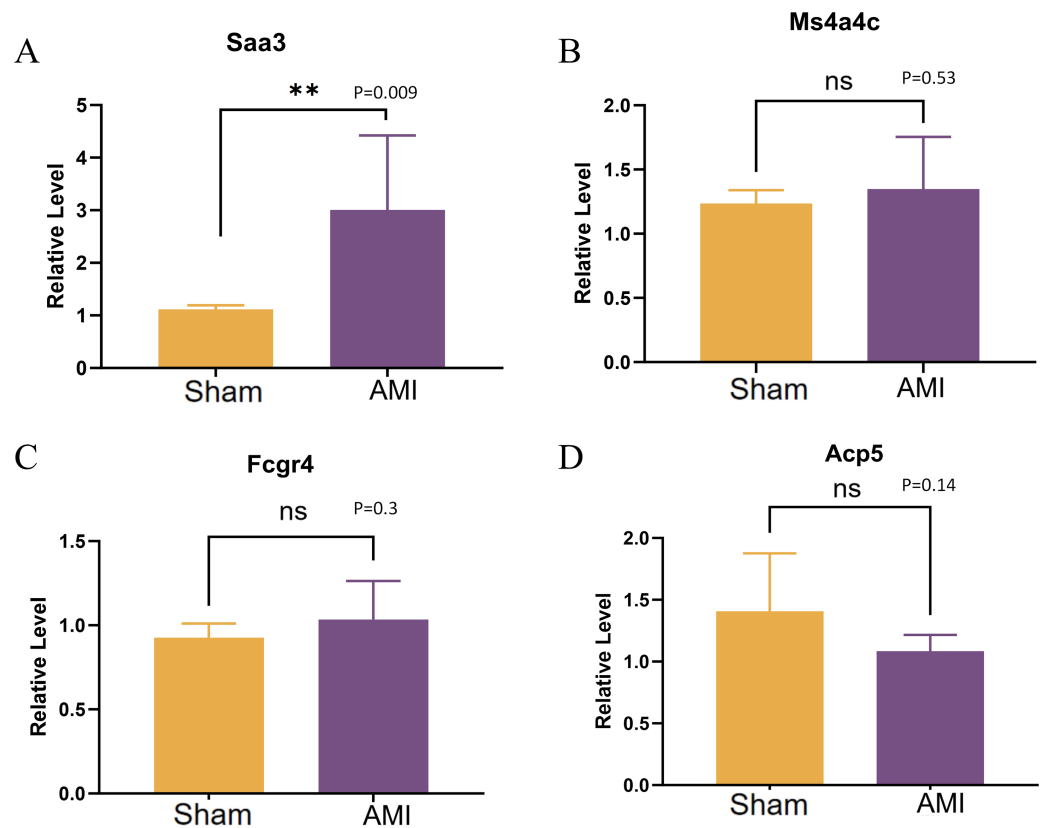
Figure 11 QRT-PCR results of key genes. (A–D) Relative expression levels of Saa3, Ms4a4c, Fcgr4, and Acp5 were detected by qRT-PCR (**$p < 0.01$, ***$p < 0.001$; ****$p < 0.0001$; ns, no significance).

Full-size 🖼 DOI: 10.7717/peerj.17981/fig-11

ACP5 has been found to function as a biomarker of systemic inflammatory load (*Chen et al., 2023*). ACP5 levels have also been found to correlate significantly with the severity of coronary atherosclerosis (*Chen et al., 2023*). Following myocardial infarction, the level of acid phosphatase (ACP) begins to rise several hours after symptom onset and lasts for 3–5 days. However, the precise mechanism underlying this phenomenon remains incompletely understood.

The Fcgr4 gene encodes the formation of fibroblast growth factor receptor 4 (FGFR4). FGFR4, also known as cluster of differentiation 334 (CD334), is an evolutionarily highly conserved tyrosine kinase. Studies indicate that fibroblast growth factor 15 (FGF15) can promote lipid oxidation and enhance glucose metabolism through FGFR4 (*Huang et al., 2007*). Additionally, FGF15 has been shown to inhibit hepatic inflammatory responses by activating FGFR 4 in septic mouse models (*Li et al., 2022*). However, the specific mechanism through which the Fcgr4 gene participates in the inflammatory response after myocardial infarction remains unclear, warranting further experimental studies for a comprehensive understanding of its role in this context.

This study presents an intriguing finding that the expression of the Saa3, Acp5, and Fcgr4 may be related to the post-AMI inflammatory response. Specifically, higher levels of

Saa3, Acp5, and Fcgr4 may be observed in mice in the AMI group, suggesting that these genes may serve as potential novel targets for intervention aimed at improving AMI.

CONCLUSION

In conclusion, this study demonstrates the involvement of Saa3, Acp5, and Fcgr4 in the inflammatory response during AMI. Our findings indicate that targeting Saa3, Acp5, and Fcgr4 may offer a promising therapeutic approach for AMI treatment in clinical settings. Saa3, Acp5 and Fcgr4 genes may be novel targets for clinical therapy of myocardial infarction.

ADDITIONAL INFORMATION AND DECLARATIONS

Competing Interests
The authors declare there are no competing interests.

Author Contributions
- Xugang Kong conceived and designed the experiments, performed the experiments, analyzed the data, prepared figures and/or tables, authored or reviewed drafts of the article, and approved the final draft.
- Guangjun Jin performed the experiments, analyzed the data, prepared figures and/or tables, authored or reviewed drafts of the article, and approved the final draft.

Animal Ethics
The following information was supplied relating to ethical approvals (*i.e.,* approving body and any reference numbers):
This study was approved by Institutional Animal Care and Use Committee of Zhejiang Center of Laboratory Animals.

Data Availability

The following information was supplied regarding data availability:

The raw data is available in the Supplemental Files.

Supplemental Information

Supplemental information for this article can be found online at http://dx.doi.org/10.7717/peerj.17981#supplemental-information.

REFERENCES

Algoet M, Janssens S, Himmelreich U, Gsell W, Pusovnik M, Van den Eynde J, Oosterlinck W. 2023. Myocardial ischemia-reperfusion injury and the influence of inflammation. *Trends in Cardiovascular Medicine* **33**(**6**):357–366 DOI 10.1016/j.tcm.2022.02.005.

Audu CO, Melvin WJ, Joshi AD, Wolf SJ, Moon JY, Davis FM, Barrett EC, Mangum KD, Deng H, Xing X, Wasikowski R, Tsoi LC, Sharma SB, Bauer TM, Shadiow J, Corriere MA, Obi AT, Kunkel SL, Levi B, Moore BB, Gudjonsson JE, Smith AM, Gallagher KA. 2022. Macrophage-specific inhibition of the histone demethylase JMJD3 decreases STING and pathologic inflammation in diabetic wound repair. *Cellular & Molecular Immunology* **19**(**11**):1251–1262 DOI 10.1038/s41423-022-00919-5.

Burke RM, Burgos Villar KN, Small EM. 2021. Fibroblast contributions to ischemic cardiac remodeling. *Cellular Signalling* **77**:109824 DOI 10.1016/j.cellsig.2020.109824.

Cai S, Zhao M, Zhou B, Yoshii A, Bugg D, Villet O, Sahu A, Olson GS, Davis J, Tian R. 2023. Mitochondrial dysfunction in macrophages promotes inflammation and suppresses repair after myocardial infarction. *Journal of Clinical Investigation* **133**(**4**):e159498 DOI 10.1172/JCI159498.

Carlson S, Helterline D, Asbe L, Dupras S, Minami E, Farris S, Stempien-Otero A. 2017. Cardiac macrophages adopt profibrotic/M2 phenotype in infarcted hearts: role of urokinase plasminogen activator. *Journal of Molecular and Cellular Cardiology* **108**:42–49 DOI 10.1016/j.yjmcc.2016.05.016.

Challa NL, Sarkar A, Kapettu S, Phanithi PB, Chakrabarti P, Parsa KVL, Misra P. 2024. TGS1/PIMT regulates pro-inflammatory macrophage mediated paracrine insulin resistance: crosstalk between macrophages and skeletal muscle cells. *Biochimica et Biophysica Acta: Molecular Basis of Disease* **1870**(**1**):166878 DOI 10.1016/j.bbadis.2023.166878.

Chen H, Xie X, Xiao H, Liang W, Lin ZJ, Lin B, Lin KY, Chen C, Guo Y. 2023. A pilot study about the role of panoptosis-based genes in atherosclerosis development. *Journal of Inflammation Research* **16**:6283–6299 DOI 10.2147/JIR.S442260.

Gong L, Wang X, Pan J, Zhang M, Liu D, Liu M, Li L, An F. 2021. The co-treatment of rosuvastatin with dapagliflozin synergistically inhibited apoptosis via activating the PI3K/AKt/mTOR signaling pathway in myocardial ischemia/reperfusion injury rats. *Open Medicine* **15**(**1**):47–57.

Huang X, Yang C, Luo Y, Jin C, Wang F, McKeehan WL. 2007. FGFR4 prevents hyperlipidemia and insulin resistance but underlies high-fat diet induced fatty liver. *Diabetes* **56(10)**:2501–2510 DOI 10.2337/db07-0648.

Jiang K, Xu LZ, Ning JZ, Cheng F. 2023. FAP promotes clear cell renal cell carcinoma progression via activating the PI3K/AKT/mTOR signaling pathway. *Cancer Cell International* **23(1)**:217 DOI 10.1186/s12935-023-03073-8.

Lee TM, Chang NC, Lin SZ. 2017. Dapagliflozin, a selective SGLT2 Inhibitor, attenuated cardiac fibrosis by regulating the macrophage polarization via STAT3 signaling in infarcted rat hearts. *Free Radical Biology and Medicine* **104**:298–310 DOI 10.1016/j.freeradbiomed.2017.01.035.

Li X, Zhu Z, Xia Z, Xu B. 2022. FGF15 protects septic mice by inhibiting inflammation and modulating treg responses. *Journal of Inflammation Research* **15**:6187–6197 DOI 10.2147/JIR.S387613.

Li Y, Dong M, Wang Q, Kumar S, Zhang R, Cheng W, Xiang J, Wang G, Ouyang K, Zhou R, Xie Y, Lu Y, Yi J, Duan H, Liu J. 2021. HIMF deletion ameliorates acute myocardial ischemic injury by promoting macrophage transformation to reparative subtype. *Basic Research in Cardiology* **116(1)**30 DOI 10.1007/s00395-021-00867-7.

Liao PD, Chen KJ, Ge JB, Zhang MZ. 2020. Clinical practice guideline of integrative chinese and western medicine for acute myocardial infarction. *Chinese Journal of Integrative Medicine* **26(7)**:539–551 DOI 10.1007/s11655-019-3154-z.

Liu Q, Sun S, Yang Z, Shao Y, Li X. 2023. Serum amyloid A 4 as a common marker of persistent inflammation in patients with neovascular age-related macular degeneration and polypoidal choroidal vasculopathy. *Journal of Inflammation Research* **16**:3783–3797 DOI 10.2147/JIR.S417791.

Liu S, Chen J, Shi J, Zhou W, Wang L, Fang W, Zhong Y, Chen X, Chen Y, Sabri A, Liu S. 2020. M1-like macrophage-derived exosomes suppress angiogenesis and exacerbate cardiac dysfunction in a myocardial infarction microenvironment. *Basic Research in Cardiology* **115(2)**:22 DOI 10.1007/s00395-020-0781-7.

Lu TC, Wu YH, Chen WY, Hung YC. 2022. Targeting oxidative stress and endothelial dysfunction using tanshinone IIA for the treatment of tissue inflammation and fibrosis. *Oxidative Medicine and Cellular Longevity* **2022**:2811789 DOI 10.1155/2022/2811789.

Lv S, Yuan P, Dong J, Lu C, Li M, Qu F, Zhu Y, Yuan Z, Zhang J. 2020. QiShenYiQi pill improves the reparative myocardial fibrosis by regulating autophagy. *Journal of Cellular and Molecular Medicine* **24(19)**:11283–11293 DOI 10.1111/jcmm.15695.

Peng H, Chen L, Deng Y, Liao X, Yang Y. 2023. Ginsenoside Rh2 mitigates myocardial damage in acute myocardial infarction by regulating pyroptosis of cardiomyocytes. *Clinical and Experimental Hypertension* **45(1)**:2229536 DOI 10.1080/10641963.2023.2229536.

R Core Team. 2020. R: a language and environment for statistical computing. Version 4.0.2. Vienna: R Foundation for Statistical Computing. *Available at https://www.r-project.org*.

Ren X, Shan WH, Wei LL, Gong CC, Pei DS. 2018. ACP5: its structure, distribution, regulation and novel functions. *Anti-Cancer Agents in Medicinal Chemistry* **18(8)**:1082–1090 DOI 10.2174/1871520618666180411123447.

Sanada Y, Yamamoto T, Satake R, Yamashita A, Kanai S, Kato N, Van de Loo FA, Nishimura F, Scherer PE, Yanaka N. 2016. Serum Amyloid A3 gene expression in adipocytes is an indicator of the interaction with macrophages. *Scientific Reports* **6**:38697 DOI 10.1038/srep38697.

Shook PL, Singh M, Singh K. 2023. Macrophages in the inflammatory phase following myocardial infarction: role of exogenous ubiquitin. *Biology* **12(9)**:1258 DOI 10.3390/biology12091258.

Thompson JC, Wilson PG, Shridas P, Ji A, De Beer M, De Beer FC, Webb NR, Tannock LR. 2018. Serum amyloid A3 is pro-atherogenic. *Atherosclerosis* **268**:32–35 DOI 10.1016/j.atherosclerosis.2017.11.011.

Venugopal H, Hanna A, Humeres C, Frangogiannis NG. 2022. Properties and functions of fibroblasts and myofibroblasts in myocardial infarction. *Cell* **11(9)**:1386 DOI 10.3390/cells11091386.

Wang K, Jin Y, Wang M, Liu J, Bu X, Mu J, Lu J. 2023. Global cardiovascular diseases burden attributable to high sodium intake from 1990 to 2019. *The Journal of Clinical Hypertension* **25(9)**:868–879 DOI 10.1111/jch.14717.

Wang N, Liu C, Wang X, He T, Li L, Liang X, Wang L, Song L, Wei Y, Wu Q, Gong C. 2019. Hyaluronic acid oligosaccharides improve myocardial function reconstruction and angiogenesis against myocardial infarction by regulation of macrophages. *Theranostics* **9(7)**:1980–1992 DOI 10.7150/thno.31073.

Wang Y, Chen Y, Zhang T. 2023. Integrated whole-genome gene expression analysis reveals an atlas of dynamic immune landscapes after myocardial infarction. *Frontiers in Cardiovascular Medicine* **10**:1087721 DOI 10.3389/fcvm.2023.1087721.

Wei Y, Xing J, Su X, Li X, Yan X, Zhao J, Tao H. 2023. IL-38 attenuates myocardial ischemia-reperfusion injury by inhibiting macrophage inflammation. *Immunity, Inflammation and Disease* **11(6)**:e898 DOI 10.1002/iid3.898.

Zhang H, Xu A, Sun X, Yang Y, Zhang L, Bai H, Ben J, Zhu X, Li X, Yang Q, Wang Z, Wu W, Yang D, Zhang Y, Xu Y, Chen Q. 2020. Self-maintenance of cardiac resident reparative macrophages attenuates doxorubicin-induced cardiomyopathy through the SR-A1-c-Myc axis. *Circulation Research* **127(5)**:610–627 DOI 10.1161/CIRCRESAHA.119.316428.

Zhuang L, Zong X, Yang Q, Fan Q, Tao R. 2023. Interleukin-34-NF-kappaB signaling aggravates myocardial ischemic/reperfusion injury by facilitating macrophage recruitment and polarization. *EBioMedicine* **95**:104744 DOI 10.1016/j.ebiom.2023.104744.